Spatial mapping of splicing factor complexes involved in exon and intron definition

Jonathan D. Ellis,[1] David Llères,[2] Marco Denegri,[2] Angus I. Lamond,[2] and Javier F. Cáceres[1]

[1]Medical Research Council Human Genetics Unit, Western General Hospital, Edinburgh EH4 2XU, Scotland, UK
[2]Wellcome Trust Biocentre, University of Dundee, Dundee DD1 5EH, Scotland, UK

We have analyzed the interaction between serine/arginine-rich (SR) proteins and splicing components that recognize either the 5′ or 3′ splice site. Previously, these interactions have been extensively characterized biochemically and are critical for both intron and exon definition. We use fluorescence resonance energy transfer (FRET) microscopy to identify interactions of individual SR proteins with the U1 small nuclear ribonucleoprotein (snRNP)–associated 70-kD protein (U1 70K) and with the small subunit of the U2 snRNP auxiliary factor (U2AF35) in live-cell nuclei. We find that these interactions occur in the presence of RNA polymerase II inhibitors, demonstrating that they are not exclusively cotranscriptional. Using FRET imaging by means of fluorescence lifetime imaging microscopy (FLIM), we map these interactions to specific sites in the nucleus. The FLIM data also reveal a previously unknown interaction between HCC1, a factor related to U2AF65, with both subunits of U2AF. Spatial mapping using FLIM-FRET reveals differences in splicing factors interactions within complexes located in separate subnuclear domains.

Introduction

A ubiquitous feature of eukaryotes is the presence of intervening sequences that interrupt coding regions of genes. Nuclear pre-mRNA splicing is the process by which these intervening sequences (introns) in mRNAs are precisely removed and the functional coding sequences (exons) ligated. Pre-mRNA splicing occurs in the spliceosome, a large RNP complex consisting of the small RNP particles (U1, U2, U4/U6, and U5 small nuclear RNPs [snRNPs]) and numerous non-snRNP splicing factors (for review see Kramer, 1996).

The spliceosome assembles de novo on the pre-mRNA in a carefully orchestrated pathway. This assembly is initiated by recognition of the 5′ and 3′ splice sites by the U1 snRNP and the heterodimeric U2 snRNP auxiliary factor (U2AF), respectively, to form the E complex (for review see Will and Luhrmann, 2001).

Binding of the U2 snRNP particle to the branch point in an ATP-dependent manner requires the auxiliary factors SF1 and U2AF and forms the A complex. U2AF65 binds to the polypyrimidine tract and contacts the branch point via its arginine/serine-rich (RS) domain (Valcarcel et al., 1996), whereas U2AF35 binds to the AG dinucleotide at the 3′ splice site (Merendino et al., 1999; Wu et al., 1999; Zorio and Blumenthal, 1999). Subsequently, recruitment of the U4/U6.U5 tri-snRNP forms the B complex, which is resolved to the catalytic C complex.

Yeast genes have very small introns, and recognition of exons seems to occur by interactions mediated across the intron itself, in a process known as intron definition (Romfo et al., 2000). The correct identification of exons is a complex problem in vertebrate genes, which have small exons separated by large introns. In this case, exon definition is facilitated by interactions between the upstream 3′ splice site and the downstream 5′ splice site (Robberson et al., 1990).

The serine/arginine-rich (SR) proteins are a highly conserved family of structurally and functionally related non-snRNP splicing factors with key roles in constitutive and alternative splicing. They have a modular domain structure consisting of one or two RNA recognition motifs (RRMs) and a C-terminal RS domain rich in arginine and serine residues (for reviews see Graveley, 2000; Sanford et al., 2005). The RRMs determine RNA binding specificity, whereas the RS domain mediates protein–protein interactions

The Rockefeller University Press $30.00
J. Cell Biol. Vol. 181 No. 6 921–934
www.jcb.org/cgi/doi/10.1083/jcb.200710051

JCB 921

and has also been shown to contact the pre-mRNA at several stages during spliceosome assembly (Shen and Green, 2004). The RS domain of SR proteins is also an important determinant of subcellular localization and nucleocytoplasmic shuttling (Caceres et al., 1997, 1998). The SR proteins are involved in multiple steps of the constitutive splicing reaction, such as promoting the recruitment of the U1 snRNP particle to the 5′ splice site (Eperon et al., 1993; Kohtz et al., 1994). They also bridge the 5′ and 3′ splice sites via RS domain–mediated interactions with the U1 70K protein (U1 snRNP-associated 70-kD protein) at the 5′ splice site and with the small subunit of the U2AF35 (U2 snRNP auxiliary factor) at the 3′ splice site (Wu and Maniatis, 1993). SR protein family members also influence splice site selection, and their activity in alternative splicing is antagonized by members of the heterogeneous nuclear RNP A/B family of proteins in a concentration-dependent manner (for review see Hastings and Krainer, 2001).

A class of related RS domain–containing proteins, termed SR-related proteins, do not always contain RRMs but are also involved in splicing regulation. This group of proteins includes the splicing coactivators SRm160/300, the U1 snRNP-associated protein U1 70K, both subunits of the U2AF splicing factor, and several tri-snRNP–specific proteins (for review see Blencowe et al., 1999). HCC1, a protein factor that is highly homologous to U2AF65, was originally identified and cloned as an autoantigen from a patient with hepatocellular carcinoma (Imai et al., 1993). It comprises two alternatively spliced isoforms termed HCC1.3 and HCC1.4, and it has been demonstrated that HCC1.3 functions as both a hormone-dependent transcriptional and splicing cofactor for steroid receptors (Dowhan et al., 2005).

There is extensive coupling among different steps in eukaryotic gene expression (for review see Maniatis and Reed, 2002). Splicing is frequently cotranscriptional and recent evidence demonstrated that the rate of transcriptional elongation affects spliceosome formation (Listerman et al., 2006) and alternative splicing (de la Mata et al., 2003). Splicing factors are distributed nonrandomly within the nucleus and are organized in the interphase nucleus in a characteristic speckled pattern (for review see Lamond and Spector, 2003). Morphological examination of speckles by electron microscopy revealed two distinct structures: granules 20–25 nm in diameter clustered in the interchromatin space, termed interchromatin granule clusters (IGCs), and fibrils ∼5 nm in diameter, termed perichromatin fibrils, which often extend from IGCs and are dispersed throughout the nucleoplasm (Spector et al., 1983). Speckles are often observed close to highly active transcription sites and specific highly active genes have been shown to localize preferentially with the periphery of speckles (Xing et al., 1993; Moen et al., 2004). Nucleotide incorporation experiments demonstrated that active sites of transcription are dispersed throughout the nucleoplasm and that the majority of actively transcribing genes are excluded from IGCs (Cmarko et al., 1999; Wei et al., 1999). Further evidence that speckles are not active sites of cotranscriptional splicing but act as storage or assembly sites for splicing factors comes from the observations that the recruitment of splicing factors to active sites of transcription can be visualized in vivo and speckles become rounded up and enlarged upon disruption of transcription or splicing (O'Keefe et al., 1994; Misteli et al., 1997).

Recent advances in imaging techniques have offered new insights into the dynamic nature of gene expression. However, because typical globular proteins are ∼5–10 nm in diameter, many such molecules can reside within the same voxel but not directly interact. To provide evidence of protein–protein interaction, it is therefore essential to measure the proximity of proteins with a resolution of ∼1–10 nm, which is simply not possible by colocalization using conventional fluorescence microscopy. This limitation imposed by the resolution of visible light can be overcome by the fluorescence resonance energy transfer (FRET) technique (or Förster resonance energy transfer; Förster, 1948). FRET is based on the ability of a donor fluorophore to transfer some of the energy from its excited state to an adjacent acceptor fluorophore, thereby reducing the amount of energy that the donor releases as fluorescence. Because the FRET energy transfer is highly distance-dependent, detection of FRET requires that the two fluorophores must be within ∼1–10 nm, i.e., the distance typically found for directly interacting proteins and consistent with being in molecular contact (Lakowicz, 1999). Thus, normally a positive FRET signal is taken to indicate a direct intermolecular interaction. In addition, for FRET to occur the donor fluorophore must have an emission spectrum overlapping the excitation spectrum of the acceptor fluorophore and the two fluorophores must be not only in close proximity but also correctly oriented. FRET can be monitored in several ways, for example, either by measuring the donor intensity (before and after acceptor photobleaching) or by measuring the decrease of donor fluorescence lifetime by fluorescence lifetime imaging microscopy (FLIM) in the presence of an acceptor (for reviews see Day et al., 2001; Wouters et al., 2001).

Many of the interactions between components of the spliceosome have been studied using in vitro techniques that perturb the temporal and spatial regulation of gene expression. FRET, detected by FLIM, allows protein–protein interactions to be studied in living cells with spatial (nanometer) and temporal resolution (for review see Wouters et al., 2001). Furthermore, FLIM-FRET can be used to quantify the percentage of interacting and noninteracting populations on a point-by-point basis at each resolved voxel within a cell.

In this paper, we use two different techniques, FRET acceptor photobleaching and FLIM-FRET to map interactions between splicing factors within living human cells with nanometer resolution. We have used this approach to demonstrate that the interactions of SR proteins with U2AF35 and U1 70K that are involved in intron and exon definition in vitro also occur in living human cells. Importantly, these interactions are maintained even in the presence of different RNA polymerase II inhibitors, such as 5,6-dichloro-1-*b*-d-ribofuranosylbenzimidazole (DRB), α-amanitin, or Actinomycin D, demonstrating that they are not exclusively cotranscriptional. In addition, we report novel interactions between HCC1 with both U2AF35 and U2AF65, suggesting a role for HCC1 in 3′ splice site selection. Importantly, use of FLIM-FRET has allowed us to identify differences in protein–protein interactions between these splicing factors in different regions of the nucleus.

A

B

C

D
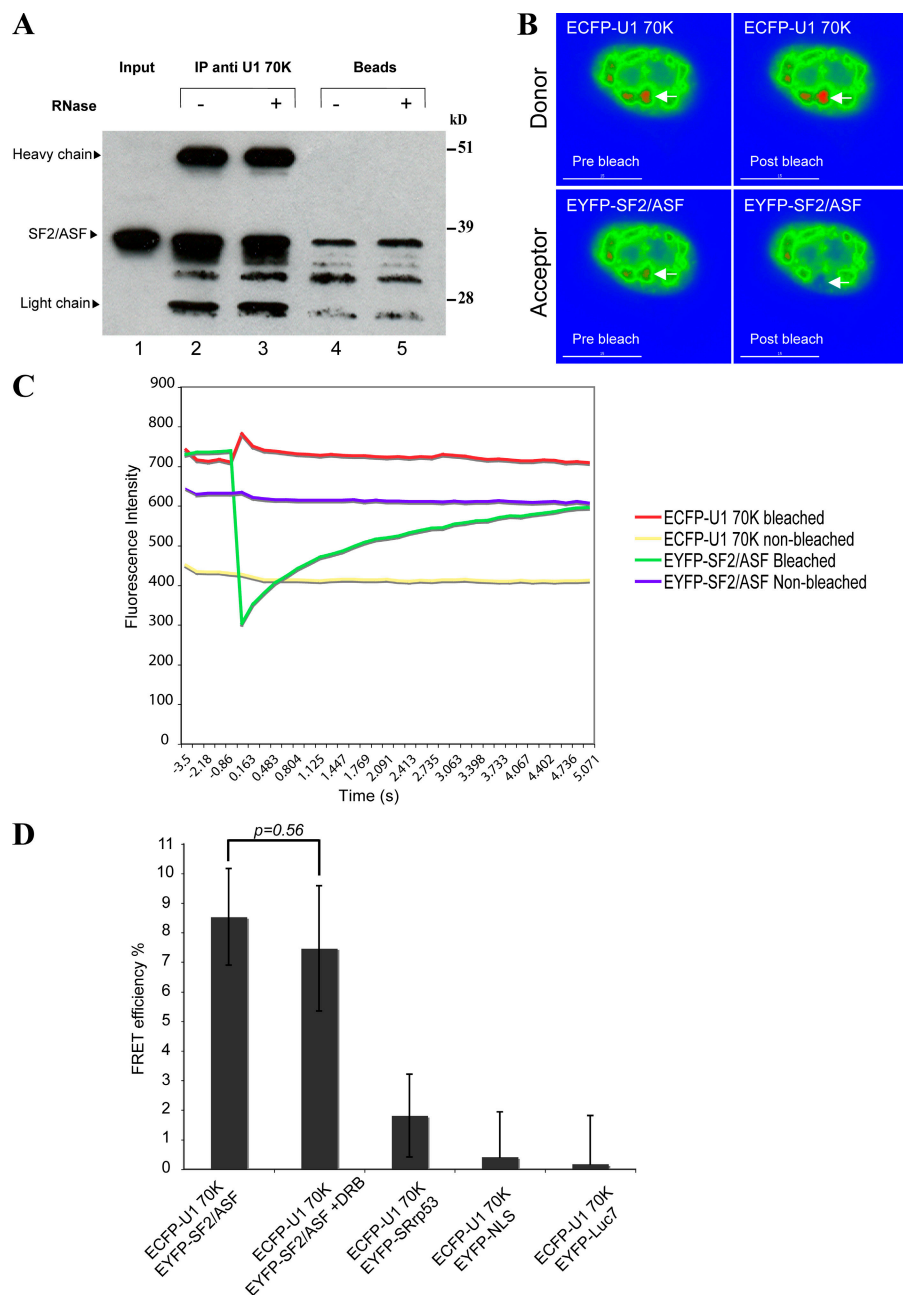
Figure 1. **U1 70K interacts with SF2/ASF in vitro and in vivo.** (A) Cell extracts prepared from 293T cells were incubated with either a mouse monoclonal anti–U1 70K antibody bound to Sepharose beads (lanes 2 and 3) or Sepharose beads alone (lanes 4 and 5). The bound proteins were analyzed by Western blotting with anti-SF2/ASF antibody. Alternatively, the assay was performed in the presence of RNase (lanes 3 and 5). (B) In vivo detection of protein–protein interactions between ECFP-U1 70K and EYFP-SF2/ASF by FRET acceptor photobleaching microscopy. HeLa cells coexpressing ECFP-U1 70K and EYFP-SF2/ASF were analyzed on a wide-field fluorescent microscope. Images were acquired before and after photobleaching. A nonbleached region similar to the bleached region (arrows) was included in the data analysis for comparison. Bars, 15 μm. (C) Donor and acceptor mean fluorescence intensities monitored in the bleached and nonbleached regions were plotted over time. (D) FRET efficiencies for the interaction between ECFP-U1 70K and EYFP-SF2/ASF in the presence and absence of DRB. A FRET efficiency for these interactions was calculated as described in Materials and methods and, when >5%, was considered significant. Plot is of FRET efficiencies ± SD (mean for 8–27 cells) between ECFP + EYFP pairs before and after DRB treatment. P-values were obtained from the two-tailed homoscedastic t test comparing the FRET efficiencies with and without DRB treatment.

Results

Splicing factor 2/alternative splicing factor (SF2/ASF) interacts with U1 70K in live cells

SF2/ASF promotes U1 snRNP recruitment to the 5′ splice site, and this effect is mediated by an interaction with the U1 snRNP-specific protein, U1 70K, that was demonstrated in far-Western and yeast two-hybrid analysis (Wu and Maniatis, 1993). First, we performed coimmunoprecipitation (co-IP) experiments of endogenous proteins to confirm their interaction in 293T cells (Fig. 1 A). Cell extracts that were immunoprecipitated with an antibody against U1 70K were probed with a monoclonal anti-SF2/ASF antibody. As shown in Fig. 1 A (compare lanes 2 and 3), U1 70K was able to pull down SF2/ASF independently of the presence of RNA.

Next, we used FRET acceptor photobleaching to study the interactions of SF2/ASF with U1 70K in living HeLa cells. In these experiments, ECFP and EYFP serve as the donor and acceptor pair for FRET, respectively. Because these experiments rely on the transient expression of epitope-tagged proteins, we first sought to determine the functionality of these fusions. There is already a large body of evidence in the literature showing that transiently expressed epitope-tagged splicing factors are indeed functional (Misteli et al., 1997; Sleeman et al., 1998; Chusainow et al., 2005). Importantly, we were able to show that the transiently expressed epitope-tagged U170K and SF2/ASF were not significantly overexpressed, with the relative abundance of the epitope-tagged proteins being similar to the level of the respective endogenous protein (Fig. S1 A, available at http://www.jcb.org/cgi/content/full/jcb.200710051/DC1). We showed that mCherry-SF2/ASF colocalizes with endogenous snRNP proteins like Sm and U2B

splicing factors in nuclear speckles (Fig. S2 A). Furthermore, we showed that both EGFP-SF2/ASF and mCherry-SF2/ASF are functional in vivo in an alternative splicing assay, as demonstrated by the fact that exogenous expression of epitope-tagged SF2/ASF caused a switch to the use of the most proximal 5′ splice site in the E1A adenoviral reporter, giving rise to the 13S isoform, as previously described (Fig. S2 B; Caceres et al., 1994).

To measure FRET by acceptor photobleaching, the donor fluorescence emission is measured, comparing the quenched with the unquenched donor emission after specific photobleaching of the acceptor fluorophore. This dequenching effect indicates an abolishment of FRET caused by photobleaching of the acceptor fluorophore, and thus confirms that the two proteins interact directly in vivo. A strong FRET signal was observed in live HeLa cells transiently coexpressing ECFP-U1 70K and EYFP-SF2/ASF after photobleaching of the acceptor (EYFP-SF2/ASF) in nuclear speckles (Fig. 1 B, arrows). This is most evident by a transient enhancement in the donor fluorescence (ECFP-U1 70K; Fig. 1, B and C) and demonstrates that these two proteins can interact in vivo. Importantly, this effect was specific because ECFP-U1 70K does not interact with an EYFP- tagged version of the second step splicing factor SRrp53 (Cazalla et al., 2005). In addition, FRET was not observed between either ECFP-U1 70K and EYFP-Luc7, a component of the U1 snRNP with a role in 5′ splice site recognition in yeast (Fortes et al., 1999), or between ECFP-U1 70K and an EYFP-tagged nuclear localization signal (EYFP-NLS; Fig. 1 D).

The interaction between U1 70K and SF2/ASF does not require ongoing transcription

Next, HeLa cells coexpressing ECFP-U1 70K and EYFP-SF2/ASF were treated with DRB to inhibit transcription and, consequently, splicing activity before analyzing the protein–protein interactions by acceptor photobleaching. DRB has been shown to interrupt the elongation step of RNA polymerase II transcription by promoting premature termination (Chodosh et al., 1989). We found that upon DRB treatment, splicing factors localized to nuclear speckles that had become enlarged and rounded (Fig. S1 C), as previously described (O'Keefe et al., 1994). Interestingly, the FRET efficiency for the interaction between ECFP-U1 70K and EYFP-SF2/ASF was similar inside the nuclear speckles after treatment with DRB (Fig. 1 D). Pulse labeling of nascent RNA with 5-Fluorouracil (5-FU) confirmed that the DRB treatment was inhibiting transcription (Fig. S1 C). Thus, the interaction of U1 70K and SF2/ASF still occurs in live cells when transcription is inhibited.

Mapping the interaction between U1 70K and SF2/ASF using FLIM

To map the localization of the U1 70K–SF2/ASF interaction within the nucleus of HeLa cells, we used FLIM. The fluorescence lifetime of EGFP–U1 70K in HeLa cells was measured, either in the presence of mCherry-C1 (negative control) or mCherry-SF2/ASF (Fig. 2 A). A FRET efficiency for the interaction of EGFP–U1 70K with mCherry-SF2/ASF was calculated as described in Materials and methods, and values >5%

were considered significant. Cotransfection of EGFP–U1 70K and mCherry-SF2/ASF resulted in a reduction of the mean donor lifetime, which is indicative of FRET. The images have been pseudocolored to show the mean fluorescence lifetime for each pixel within the cell and the percentage of FRET efficiency (Fig. 2 A). It can be seen that FRET between EGFP–U1 70K and mCherry-SF2/ASF occurs to a greater extent in the speckles (Fig. 2, A [arrowheads] and C) than in the nucleoplasm (Fig. 2, A [arrows] and C).

In addition, we resolved the fractional contribution of the FRET species for each pixel through the nuclei by calculating the FRET amplitude percentage (see Materials and methods). A higher FRET population of EGFP–U1 70K was observed in the nuclear speckles as compared with the nucleoplasm compartment (Fig. 2 A, FRET amplitude %). It was also important to demonstrate that a higher abundance of splicing factors in the speckles did not lead to false positives. There has been no prior biochemical evidence to suggest a direct interaction between U1 70K and U2AF35. Instead, it was proposed that SR proteins bridge these factors (Wu and Maniatis, 1993). This provided a negative control that could be analyzed by FLIM-FRET. As expected, cotransfection of EGFP-U1 70K and mCherry-U2AF35 resulted in no significant FRET (Fig. 2 C and Fig. S3, available at http://www.jcb.org/cgi/content/full/jcb.200710051/DC1). These data demonstrate that there is a greater interaction between the U1 70K and SF2/ASF proteins within the speckles than in the diffuse nucleoplasmic pool and that the proportion of complexes containing U1 70K interacting with SF2/ASF is higher within the speckles. We further demonstrated that the high local concentration of fluorescently tagged proteins in the speckles is not alone sufficient to induce FRET.

The localization of the U1 70K–SF2/ASF interaction in transcriptionally repressed cells

Several lines of evidence point to speckles functioning as storage/assembly/modification compartments that can supply splicing factors to active transcription sites (Misteli, 2000). Therefore, we determined whether treatment with the transcriptional inhibitor DRB affected the localization of the interaction between EGFP–U1 70K and mCherry-SF2/ASF. Upon cotransfection of EGFP–U1 70K and mCherry-SF2/ASF and subsequent treatment with DRB, images captured by FLIM microscopy revealed a strong FRET signal, which was stronger in the enlarged and rounded speckles (Fig. 2 B, arrowheads). The fluorescence lifetime and the FRET efficiency variations between the speckles and nucleoplasm compartments were also analyzed for a population of DRB-treated cells and compared with untreated cells. From this analysis, we concluded that there was not a major change in the total nuclear FRET efficiency between EGFP–U1 70K and mCherry-SF2/ASF after DRB treatment as measured by FLIM. Similar results were obtained upon inhibition of RNA polymerase II transcription with other inhibitors, including α-amanitin and Actinomycin D (Fig. S4, available at http://www.jcb.org/cgi/content/full/jcb.200710051/DC1). However, from the spatiotemporal resolution of the interactions revealed by using
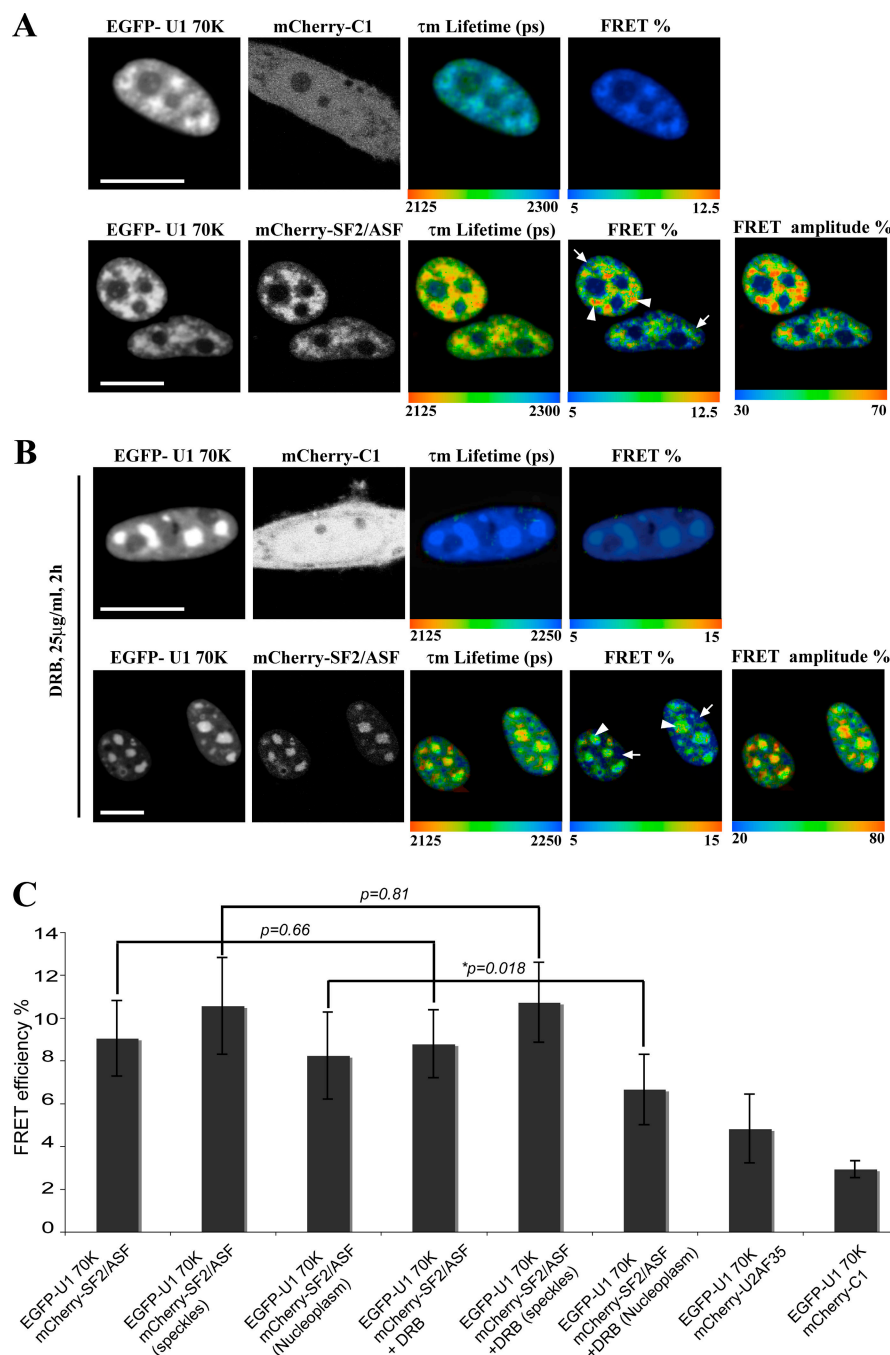
Figure 2. **Spatial mapping of the interaction of U1 70K with SF2/ASF in vivo.** (A) HeLa cells were transfected with EGFP–U1 70K and cotransfected with either mCherry-C1 or mCherry-SF2/ASF. Shown are confocal images of transfected cells and FLIM images of the same cells, in which mean fluorescence lifetime is shown in pseudocolor. The color scale with the respective lifetimes (in picoseconds [ps]) is indicated. The percentage of FRET efficiencies and FRET amplitude are shown in continuous pseudocolor. The color scale with the respective FRET efficiencies (percentage) is indicated. The FRET amplitude % represents the fraction of interacting donor molecules, also defined as the FRET population % (or concentration of FRET species). (B) FRET between U1 70K and SF2/ASF, in the presence of DRB, measured by FLIM. Experiments were performed exactly as described for A, except cells were treated with 25 µg/ml of DRB for 2 h before images were taken. Bars, 10 µm. (C) FRET efficiencies calculated from FLIM measurements for the interaction of SF2/ASF with U1 70K in the presence and absence of DRB. Plot is of mean FRET efficiencies ± SD for 9–20 cells. To measure the FRET efficiency in the speckles and nucleoplasm, a region characteristic of each was selected for each cell. P-values were obtained as described in the Fig. 1 legend. *, P < 0.1.

the FLIM-FRET technique, a decrease in the FRET efficiency specifically in the nucleoplasm was observed in the presence of DRB (P = 0.018; Fig. 2, B [arrows] and C). Furthermore, the proportion of interacting EGFP–U1 70K was also significantly reduced in the nucleoplasm. This suggests that upon inhibition of transcription, the interactions between splicing factors may be inhibited at nucleoplasmic sites of transcription and splicing.

SF2/ASF interacts with U2AF35 in live cells

The interaction between U2AF35 and individual SR proteins is proposed to play two important roles in the cell. First, SR proteins bound to exonic splicing enhancers interact with U2AF35 to promote complex assembly at the 3′ splice site (Zuo and Maniatis, 1996; Graveley et al., 2001). Second, it has been proposed that SR proteins can interact simultaneously with U2AF35 and U1 70K, thereby bridging factors assembled on both 5′ and 3′ splice sites (Wu and Maniatis, 1993). This bridging can occur either across the exon or the intron and is therefore proposed to play a role in exon and intron definition.

First, we performed Co-IP experiments of 293T cells transiently expressing EGFP-U2AF35 to confirm this biochemical interaction. Cell extracts that were immunoprecipitated with an antibody against EGFP were revealed with a monoclonal anti-SFS/ASF antibody. As shown in Fig. 3 A (lanes 3 and 4),

Figure 3. EGFP-U2AF35 interacts with SF2/ASF in cultured mammalian cells. (A) Cell extracts prepared from 293T cells either transiently transfected with EGFP-U2AF35 (lanes 3 and 4) or mock transfected (lanes 5 and 6) were incubated with anti-GFP antibody bound to Sepharose beads. The bound proteins were analyzed by Western blotting with an anti-SF2/ASF antibody. Alternatively, the assay was performed in the presence of RNase (lanes 4 and 6). NTC, nontransfected cells. (B) Effect of DRB on the interaction between ECFP-U2AF35 and EYFP-SF2/ASF. Plot is of FRET efficiencies ± SD (mean for 9–27 cells) between ECFP + EYFP fusion pairs before and after DRB treatment. P-values were obtained as described in the Fig. 1 legend.
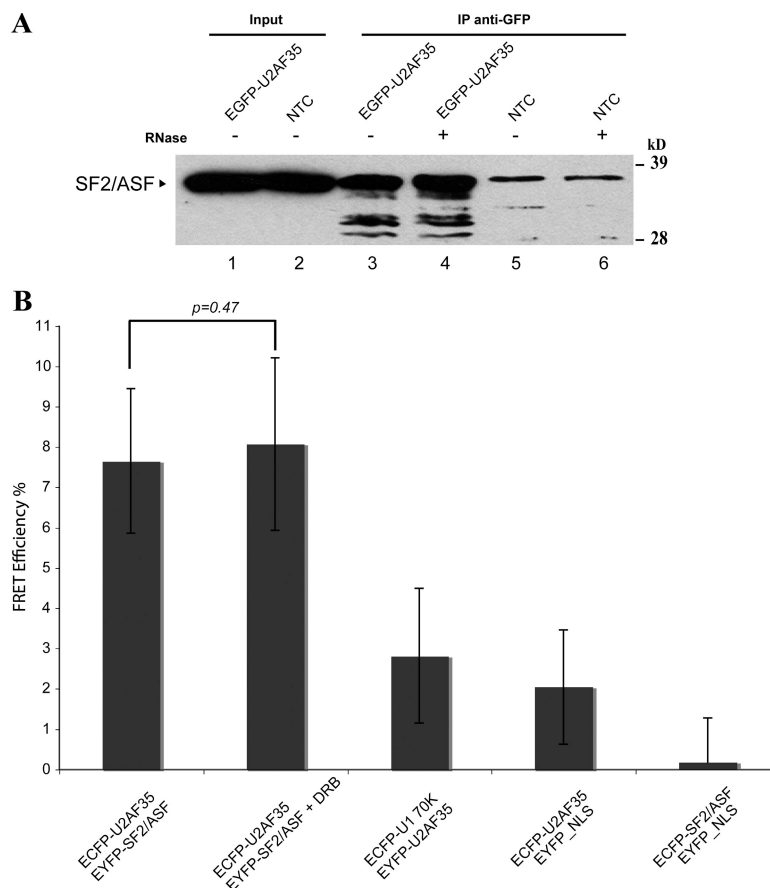
EGFP-U2AF35 was able to pull down SF2/ASF independently of the presence of RNA.

Next, we analyzed the interaction between U2AF35 and SF2/ASF by FRET acceptor photobleaching. HeLa cells were cotransfected with ECFP-U2AF35 and EYFP-SF2/ASF and the donor intensities were monitored before and after photobleaching of the acceptor to calculate a FRET efficiency for this interaction. FRET between ECFP-U2AF35 and EYFP-SF2/ASF was observed and this interaction was not prevented by DRB treatment (Fig. 3 B). Importantly, this interaction was specific because little or no FRET was observed either between U2AF35 and U1 70K or upon cotransfection with EYFP_NLS (Fig. 3 B).

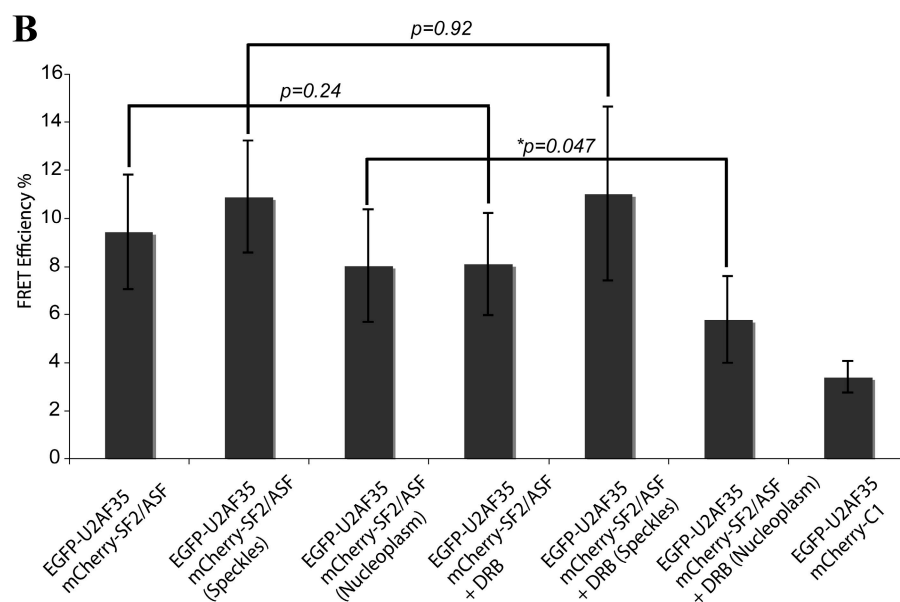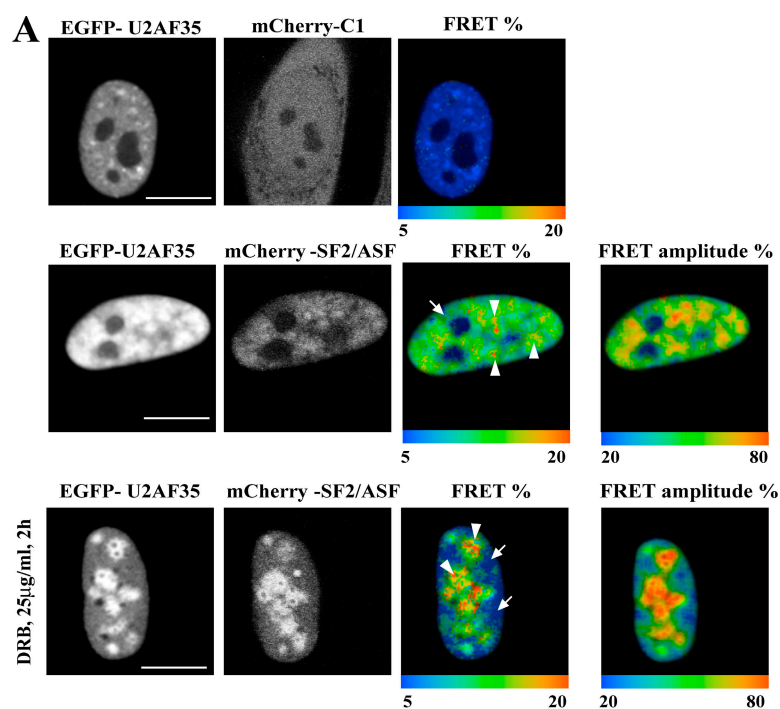## The interaction between U2AF35 and SF2/ASF occurs predominantly in speckles

The intracellular distribution of the interactions between EGFP-U2AF35 and mCherry-SF2/ASF was mapped using FLIM-FRET. Cotransfection of EGFP-U2AF35 and mCherry-SF2/ASF resulted in a reduction of the mean donor fluorescence lifetime. The pseudocolored images depicting the FRET efficiencies in continuous color demonstrated that mCherry-SF2/ASF interacts with EGFP-U2AF35 in a similar pattern to that observed for its interaction with EGFP-U1 70K (Fig. 4 A). Indeed, although a significant FRET signal was observed in the nucleoplasm (Fig. 4 A, arrows), the strongest regions of FRET were observed locally in speckles (Fig. 4 A, arrowheads). These observations were confirmed when the FRET efficiencies were averaged over a population of cells (Fig. 4 B). By calculating

the FRET amplitude percentage (see Materials and methods), we also found that the concentration of EGFP-U2AF35 proteins interacting with mCherry-SF2/ASF is much higher inside the nuclear speckles (~80%) than in the nucleoplasm (~50%) in untreated cells (Fig. 4 A, middle, FRET amplitude %).

Upon inhibition of transcription with DRB, α-amanitin, or Actinomycin D (Fig. S4), the FRET efficiency between EGFP-U2AF35 and mCherry-SF2/ASF measured in nuclear speckles by FLIM was not significantly affected (Fig. 4 A, bottom, arrowheads). In contrast, a decrease of FRET was observed in the nucleoplasmic compartment surrounding the speckles after inhibition of the transcription (Fig. 4 A, bottom, arrows; Fig. 4 B, P = 0.047). Furthermore, the fraction of EGFP-U2AF35 interacting with mCherry-SF2/ASF and present in the nucleoplasm after treatment was significantly reduced (~20%).

Several SR proteins interact with U1 70K and U2AF35

In vitro experiments have previously shown that both SF2/ASF and SC35 are capable of interacting with U1 70K and U2AF35 (Wu and Maniatis, 1993). We have extended these observations to show that both SC35 and SRp20 interact with U1 70K and U2AF35 in live HeLa cells. The FRET efficiencies obtained from the acceptor photobleaching analysis of these interactions are shown in Fig. 5 A. We also found that DRB does not reduce the FRET efficiencies for the interaction of SC35 with U1 70K or U2AF35.
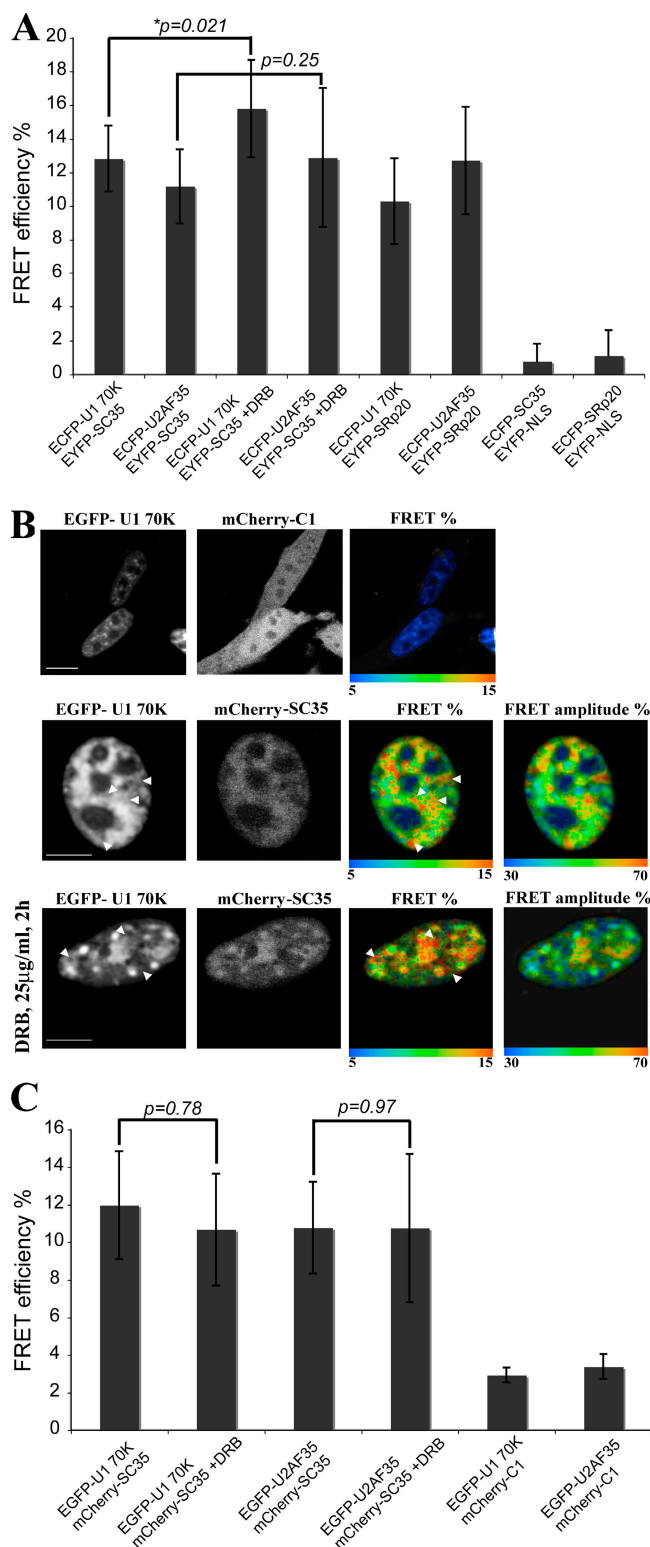
A

EGFP- U2AF35   mCherry-C1   FRET %

EGFP-U2AF35   mCherry -SF2/ASF   FRET %   FRET amplitude %

EGFP- U2AF35   mCherry -SF2/ASF   FRET %   FRET amplitude %

DRB, 25μg/ml, 2h

B

Figure 4. **FRET between U2AF35 and SF2/ASF measured by FLIM.** (A) HeLa cells were cotransfected with EGFP-U2AF35 and either mCherry-C1 or mCherry-SF2/ASF. Confocal images are of transfected cells and FLIM images of the same cells, in which FRET efficiency and FRET amplitude are shown in pseudocolor. The color scale with the respective efficiency (%) is indicated. Top, EGFP-U2AF35 + mCherry-C1; Middle, EGFP-U2AF35 + mCherry-SF2/ASF; Bottom, EGFP-U2AF35 + mCherry-SF2/ASF in the presence of DRB. Bars, 10 μm. (B) FRET efficiencies determined by FLIM for interaction of SF2/ASF with U2AF35 in the presence and absence of DRB. Plot is of mean FRET efficiencies ± SD for seven to nine cells. To measure the FRET efficiency in the speckles and nucleoplasm, a region characteristic of each was selected for each cell. P-values were obtained as described in the Fig. 1 legend. *, $P < 0.1$.

FLIM-FRET was used to map the protein–protein interaction sites of mCherry-SC35 with EGFP-U1 70K and EGFP-U2AF35. We observed that the highest FRET efficiencies do not correspond only with regions of speckles, as was the case with SF2/ASF, but are instead also observed in areas of the nucleoplasm adjacent to the nuclear speckles (Fig. 5 B, middle, arrowheads). Interestingly, these areas where the strongest FRET is taking place are not identical to the regions showing the highest population of EGFP-U1 70K interacting with mCherry-SF2/ASF (Fig. 5 B, middle, FRET amplitude %), but likely represent a subpopulation of proteins involved in these interactions. A similar pattern was observed upon treatment with DRB, making it unlikely that these regions of high FRET correspond to major sites of ongoing transcription and splicing.

HCC1 interacts with both U2AF35 and U2AF65

HCC1 is an SR-related protein that is highly similar to U2AF65, although its possible role in constitutive splicing is unclear (Dowhan et al., 2005). We previously found that HCC1 interacts with the second step splicing factor SRrp53 (Cazalla et al., 2005). It has been proposed that HCC1 interacts with components at the 3′ splice site, possibly replacing U2AF65 at the polypyrimidine tract and forming a U2AF-like complex with U2AF35. Moreover, several factors related to U2AF35 have been characterized in mammalian cells, suggesting the existence of multiple U2AF-like complexes (Tronchere et al., 1997; Shepard et al., 2002).

We have characterized the protein interaction partners of HCC1 by Co-IP experiments and subsequently by FRET

Figure 5. **SRp20 and SC35 interact with U1 70K and U2AF35.** (A) Plot of FRET efficiencies ± SD (mean for 7–14 cells) between ECFP and EYFP fusion proteins measured by FRET acceptor photobleaching. P-values were obtained from the *t* test comparing the FRET efficiencies with and without DRB treatment. (B) FRET between U1 70K and SC35 measured by FLIM. HeLa cells were transfected with EGFP-U1 70K and cotransfected with either mCherry-C1 or mCherry-SC35. Confocal images are of transfected cells and FLIM images are of the same cells, in which FRET efficiency and FRET amplitude are shown in pseudocolor. The color scale with the respective efficiency (%) is indicated. Top, EGFP-U1 70K + mCherry-C1; Middle, EGFP-U1 70K + mCherry-SC35; Bottom, EGFP-U1 70K + mCherry-SC35

microscopy. First, EGFP-U2AF35 was shown to be capable of pulling down T7-tagged HCC1.4 in Co-IP assays performed in 293T cells (Fig. 6 A). The hypothesis that HCC1 may form an alternative U2AF-like complex with U2AF35 was challenged by the observation that HCC1 can pull down both U2AF35 and U2AF65 in Co-IP assays (Fig. 6, A and B). Furthermore, this interaction addressed by Co-IP remains after Rnase treatment (Fig. 6, A [lanes 3 and 4] and B [lanes 2 and 4]).These data suggest that HCC1 interacts with the U2AF heterodimer in an RNA-independent manner, although it is still possible that HCC1-U2AF35 and HCC1-U2AF65 complexes exist within the cell.

We have further characterized the protein–protein interactions of HCC1 by FRET acceptor photobleaching. Cotransfection of ECFP-HCC1 and either EYFP-U2AF35, or EYFP-U2AF65 resulted in a FRET signal that was not significantly altered upon DRB treatment (Fig. 6 C). As previously demonstrated by acceptor photobleaching assays (Chusainow et al., 2005), we did not observe any self-interaction of U2AF65 (Fig. 6 C).
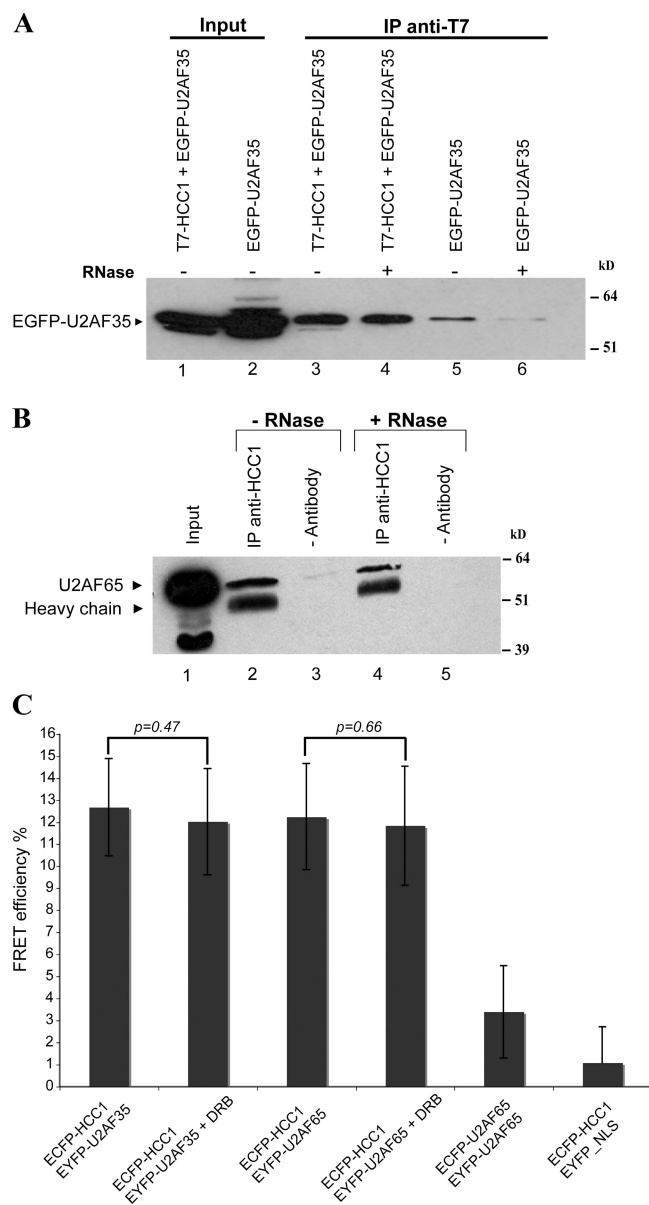
The subnuclear localization of protein–protein interactions between EGFP-HCC1 and either mCherry-U2AF35 or mCherry-U2AF65 was mapped using FLIM-FRET. The regions of highest FRET for the interaction of EGFP-HCC1 with mCherry-U2AF35 were not confined to speckles, as was previously observed for the interactions involving SF2/ASF (Fig. 7 A, middle, arrows). For the interaction of EGFP-HCC1 with mCherry-U2AF65, the regions of highest FRET occurred within discrete domains within the nucleoplasm rather than within speckles (Fig. 7 B, middle). Interestingly, these regions of high FRET persisted within the nucleoplasm upon treatment with DRB (Fig. 7 B, bottom, arrowheads [high FRET domain] and arrows [splicing speckles]). In contrast, no significant FRET was observed between EGFP-U2AF65 and mCherry-U2AF65 as judged by FLIM (unpublished data). Collectively, these results show that HCC1 can interact with both subunits of the U2AF heterodimer and strongly suggest that distinct complexes of splicing factors accumulate in different regions within the nucleus.

Discussion

Protein–protein interactions involved in spliceosome assembly have been studied extensively in the past, mainly using in vitro techniques and yeast two-hybrid analysis. However, the advent of FRET microscopy has made it possible to study molecular interactions between splicing factors in live cells, thereby avoiding perturbing the highly structured dynamic nature of the nucleus or introducing artificial salt concentrations, as is common with in vitro approaches. The importance of studying protein–protein interactions in live cells is self-evident and is demonstrated by previous work that showed that co-IP does not always recapitulate the in vivo state of ribonucleoprotein complexes because of reassociation of molecules subsequent to cell lysis (Mili and Steitz, 2004).
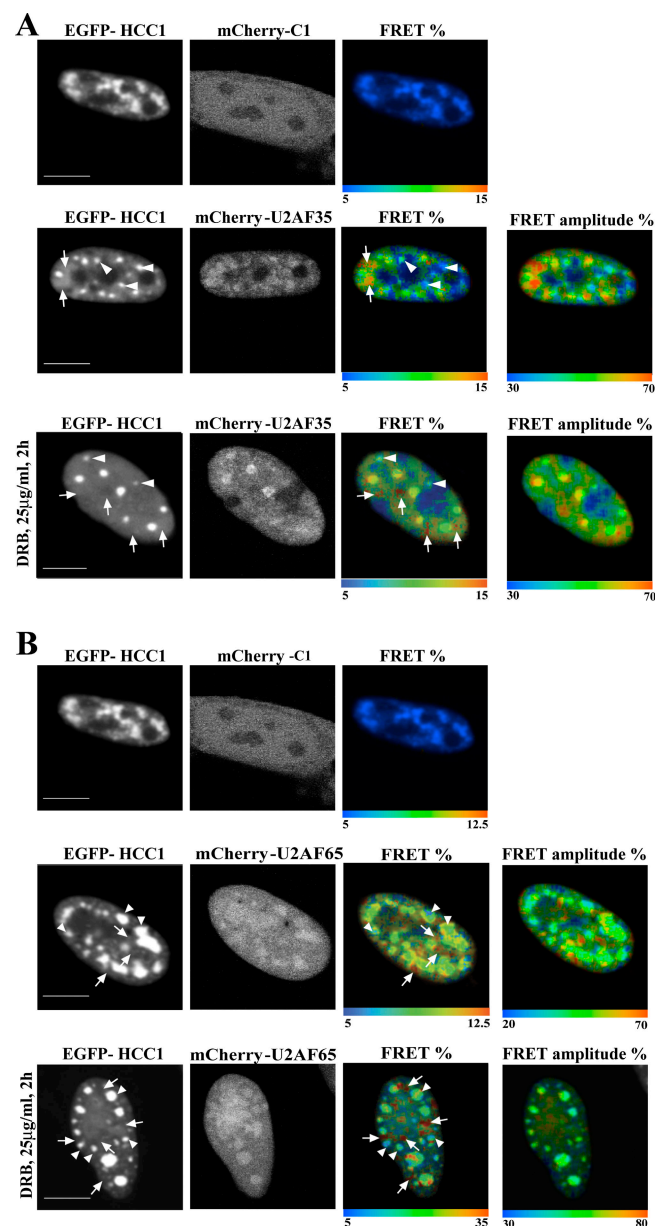
in the presence of DRB. Arrowheads indicate high FRET within the nucleoplasm. Bars, 10 µm. (C) FRET efficiencies determined by FLIM for interaction of SC35 with U1 70K and U2AF35 in the presence and absence of DRB. Plot is of mean FRET efficiencies ± SD for 8–11 cells. P-values were obtained as described in A.

A

Input | IP anti-T7

EGFP-U2AF35 ▶

kD
— 64
— 51

1 2 3 4 5 6

B

- RNase | + RNase

U2AF65 ▶
Heavy chain ▶

kD
— 64
— 51
— 39

1 2 3 4 5

C

Figure 6. **HCC1 interacts with both subunits of the U2AF heterodimer in vitro and in vivo.** (A) Extracts prepared from 293T cells transiently transfected with either EGFP-U2AF35 and pCG-T7-HCC1.4 (lanes 3 and 4) or EGFP-U2AF35 (lanes 5 and 6) were incubated with anti-T7 antibody bound to Sepharose beads. The bound proteins were analyzed by Western blotting with anti-GFP antibody. Alternatively, the assay was performed in the presence of RNase (lanes 4 and 6). (B) U2AF65 interacts with HCC1 in cultured mammalian cells. Extracts prepared from 293T were incubated with either anti-HCC1 antibody bound to Sepharose beads (lanes 2 and 4) or Sepharose beads alone (lanes 3 and 5). The bound proteins were analyzed by Western blotting with anti-U2AF65 antibody. Alternatively, the immunoprecipitate was treated with RNase (lanes 4 and 5). (C) Effect of DRB on interactions of HCC1 with U2AF35 and U2AF65. Plot is of FRET efficiencies ± SD (mean for 8–18 cells) between ECFP and EYFP fusion proteins measured by FRET acceptor photobleaching. P-values were obtained as described in the Fig. 5 legend.

Figure 7. **FRET between HCC1 and both subunits of the U2AF heterodimer measured by FLIM.** (A) HeLa cells were cotransfected with EGFP-HCC1 and either mCherry-C1 or mCherry-U2AF35. Confocal images are of transfected cells and FLIM images are of the same cells. The color scale with the respective efficiency (%) is indicated. The FRET efficiencies are shown in continuous pseudo-color. Top, EGFP-HCC1 + mCherry-C1; Middle, EGFP-HCC1 + mCherry-U2AF35; Bottom, EGFP-HCC1 + mCherry-U2AF35 in the presence of DRB. Arrows indicate high FRET within the nucleoplasm and arrowheads indicate nuclear speckles. (B) FRET between HCC1 and U2AF65 measured by FLIM. HeLa cells were transfected with EGFP-HCC1 and cotransfected with either mCherry-C1 or mCherry-U2AF65. Confocal images are of transfected cells and FLIM images are of same cells, in which the percentage of FRET Efficiency and FRET amplitude are shown in pseudocolor. The color scale with the respective efficiency (%) is indicated. Top, EGFP-HCC1 + mCherry-C1; Middle, EGFP-HCC1 + mCherry-U2AF65; Bottom, EGFP-HCC1 + mCherry-U2AF65 in the presence of DRB. Arrowheads indicate high FRET within the nucleoplasm and arrowheads indicate nuclear speckles. Bars, 10 μm.

FRAP analysis has shown that splicing factors are highly dynamic and shuttle rapidly between speckles and the nucleoplasm on a time scale of seconds (Phair and Misteli, 2000). Therefore, these highly dynamic and abundant factors may be constantly associating and disassociating with each other within the nucleus.

It remains to be determined how the distribution and formation of splicing factor complexes are regulated within the cell. In this paper, we demonstrate for the first time that different complexes of splicing factors show differential distributions in live cell nuclei.

Table I. **Summary of protein interactions and FRET efficiencies analyzed by FLIM in nucleoplasm and nuclear speckles in the absence or presence of an inhibitor of transcription**

Interaction partners	Transcription		Transcription inhibition	
	Nucleoplasm	Speckles	Nucleoplasm	Speckles
U1 70K–SF2/ASF	++	+++	−	+++
U1 70K–SC35	+++	++	++	+++
U1 70K–U2AF35	−	−	−	−
U2AF 35–SF2/ASF	++	+++	−	+++
U2AF 35–SC35	+++	++	++	+++
HCC1–U2AF35	++	+	++	++
HCC1–U2AF65	++	+	+++	++

The + and − represent the strength of the protein interactions. +++, strong interaction; ++, moderate interaction; +, weak interaction; −, no interaction.

FRET analysis of splicing factor complexes

The role of different subnuclear compartments within the mammalian cell nucleus has been investigated previously by studying the colocalization of protein factors with a variety of nuclear bodies. For example, splicing snRNPs associate with Cajal bodies, likely as part of a nuclear snRNP assembly pathway (Lamond and Sleeman, 2003). Both snRNPs and protein splicing factors also concentrate in speckles and the nucleoplasm, and these regions are differentially affected upon inhibition of transcription. Thus, blocking transcription causes splicing factors to relocate from the nucleoplasm and concentrate in enlarged speckles (for review see Lamond and Spector, 2003). FRET microscopy makes it possible to distinguish between factors that simply reside in the same compartments and those that directly interact with each other. The FRET interaction is strongly distance dependent. Thus, FRET reveals direct intermolecular interactions. (Patterson et al., 2000). However, FRET also is highly dependent on fluorophore orientation. Thus, absence of FRET could mean either that no direct interaction occurs or that some remodeling event of the protein complex occurs that alters the protein orientation. In the case of FRET measurements by FLIM, as used in this study, individual interactions are detected on a nanosecond time scale using a pulsed laser source. Typically, interactions are recorded for ∼120 s, and all the separate interactions detected during this period are integrated to provide a map of the steady-state distribution of protein interactions in a pixel-by-pixel basis throughout the 2D area of the cell. Furthermore, the FLIM data also allow details of the fraction of protein involved in FRET interactions to be calculated. This approach thus provides a highly detailed view on the spatial organization of protein–protein interactions within live cells.

In this paper, we have used FRET acceptor photobleaching and FLIM-FRET to study a variety of splicing factor complexes. The existence of splicing complexes previously isolated in vitro has been confirmed in living cells, and we have also used this technique to identify novel splicing complexes. The SR proteins SF2/ASF and SC35 have previously been shown to interact with U1 70K and U2AF35 by in vitro approaches (Wu and Maniatis, 1993; Kohtz et al., 1994). Therefore, it was proposed that SR proteins play a role in exon and intron definition by interacting with U1 70K bound at the 5′ splice site and U2AF35 bound at the 3′ splice site. We have used FRET microscopy to demonstrate that the SR proteins SF2/ASF and SC35 interact with both U1 70K and U2AF35. We have also extended the original in vitro studies to show that another SR protein family member, SRp20, also interacts with U1 70K and U2AF35. Thus, the ability of SR proteins to interact with components at the 5′ and 3′ splice site in live HeLa cells is not confined to SF2/ASF. These FLIM/FRET results were also recapitulated in cells after 3.7% PFA fixation (Fig. S5, available at http://www.jcb.org/cgi/content/full/jcb.200710051/DC1).

Subcellular distribution of splicing complexes

The subcellular distribution of protein–protein interactions has been mapped at nanometer resolution using a FLIM-FRET approach. Interestingly, we found that these protein–protein interactions have a differential distribution within the nucleus. Although interactions involving SF2/ASF localized preferentially to the nuclear speckles, those involving SC35 preferentially localized to the nucleoplasm (Table I). We observed that most of the interactions of SR proteins with either U1 70K or U2AF35 occur in both the nuclear speckles and the nucleoplasm, even in transcriptionally repressed cells. The protein–protein interactions between U2AF35 and U2AF65 have previously been studied by FRET acceptor photobleaching (Chusainow et al., 2005), and also, in this case, inhibition of transcription by DRB had little or no effect on the FRET efficiency observed for this interaction. The fact that inhibition of transcription, which removes production of new splicing substrates, did not prevent the observed interactions suggests that they are not exclusively cotranscriptional or at least do not strictly require ongoing nascent transcription. Interestingly, a FRET microscopy approach has revealed that the splicing factors SF1 and U2AF, which participate in the recognition of the 3′ splice site, associate in extraspliceosomal complexes that persist upon inhibition of transcription (Rino et al., 2008).

Numerous pieces of evidence suggest that speckles are not major active sites of splicing but may act as either storage or assembly sites for splicing factors. The increased FRET efficiency observed in speckles upon treatment with either DRB or other transcriptional inhibitors is consistent with the idea that splicing factors involved in intron and exon definition associate together in a complex before being recruited cotranscriptionally to the spliceosome. Furthermore, when FRET efficiencies were measured in the nucleoplasm by FLIM-FRET, a significant decrease in the FRET efficiency for SF2/ASF with U1 70K and

U2AF35 was observed. This is particularly interesting, as it suggests that the interactions between splicing factors are reduced, but not abolished, at active sites of splicing upon inhibition of transcription. Another interesting possibility is that the reduced FRET efficiency reflects structural remodeling of the splicing complexes at these sites, which affects the protein orientation geometry.

Further evidence that SR proteins and U1 70K associate with each other before they are recruited cotranscriptionally to the spliceosome has come from studies of factors associated with RNA polymerase II. A comprehensive proteomic analysis of immunopurified human RNA polymerase II identified >100 specifically associated proteins (Das et al., 2007). Among these are the SR proteins and all the components of the U1 snRNP but no other snRNP proteins or splicing factors. This has led to a model being proposed whereby the association of U1 snRNP and SR proteins with RNA polymerase II results in their cotranscriptional recruitment to nascent transcripts to promote spliceosome assembly (Das et al., 2007). Moreover, splicing efficiency is strongly enhanced if SR proteins are available during transcription but not if they are added immediately after transcription. Our in vivo FRET studies are consistent with this model.

Splicing factors involved in recognition of the 3′ splice site

The role of HCC1, a factor highly related to U2AF65, in constitutive splicing is poorly understood. An alternatively spliced isoform of HCC1, termed HCC1.3, was purified as a spliceosome component capable of affecting the splicing reaction (Rappsilber et al., 2002) and has been shown to regulate both transcription and alternative splicing in a steroid hormone–dependent manner (Dowhan et al., 2005). An alternative isoform of HCC1, termed HCC1.4, interacts with an SR-related protein, SRrp53, which can activate weak 3′ splice sites (Cazalla et al., 2005). A second U2AF65-like component, PUF60, which binds to the polypyrimidine tract and regulates the alternative splicing of a subset of exons, has been identified (Page-McCaw et al., 1999; Hastings et al., 2007). All three proteins, i.e., U2AF65, PUF60, and HCC1, have been shown to interact with SRp54, which has been implicated in early 3′ splice site recognition (Zhang and Wu, 1996). This has led to the proposal that U2AF65-like factors can interact with components required for the early recognition of the 3′ splice site and influence the commitment to splicing.

A U2AF35-related protein, termed Urp, interacts with U2AF65 through a U2AF35 homologous region and with SR proteins through its RS domain (Troncheré et al., 1997). Coimmunodepletion showed that Urp is associated with the U2AF heterodimer and does not form an alternative U2AF-like complex with U2AF65. It has been proposed that Urp and U2AF35 independently position RS domain–containing factors within spliceosomes. In contrast, a second U2AF35-like factor, U2AF26, interacts with U2AF65 and can functionally substitute for U2AF35 in both constitutive and enhancer-dependent splicing (Shepard et al., 2002). Therefore, distinct U2AF-like complexes can function in pre-mRNA splicing. The observation that HCC1 can interact both with the U2AF heterodimer and with SR-related proteins suggests that HCC1 may play a similar role to Urp in spliceosome

assembly. Further investigation will be required to determine whether HCC1 interacts directly with U2AF26, U2AF35, U2AF65, or Urp. It also remains to be determined whether HCC1 plays a role in binding to the polypyrimidine tract and whether it is recruited to a subset of pre-mRNA substrates.

In vitro experiments have shown that the phosphorylation status of splicing factors is important for regulating the assembly and disassembly of the spliceosome (Tazi et al., 1993; Mermoud et al., 1994). Furthermore, phosphorylation of SF2/ASF has been shown to increase its affinity for U1 70K (Xiao and Manley, 1997). Future FRET analyses could be used to determine the effects of modulating either signaling pathways and/or kinase activity on the regulation of interactions between splicing factors in live cells.

In summary, we have used FRET acceptor photobleaching and FLIM-FRET to characterize the interactions involved in exon and intron definition in living HeLa cells, to quantify the fraction of splicing factors proteins involved in these interactions, and to map their subnuclear distribution. FLIM data demonstrates that the formation of splicing factor complexes is not exclusively regulated by the abundance of individual components, as the highest FRET efficiencies did not always occur in regions where splicing factors concentrate.

Materials and methods

Plasmid constructs
Human U1 70K and Luc7A were cloned by reverse transcription from total RNA from HeLa cells. Total RNA was prepared using TriReagent (Sigma-Aldrich) according to the manufacturer's specifications. 5 µg of total RNA was used for synthesis of first-strand cDNA with Super Script II RNase H⁻ reverse transcription (Invitrogen) according to the manufacturer's protocol, and 10% of the cDNA obtained in each case was used for PCR amplification. Fragments corresponding to full-length coding sequence of human U1 70K or Luc7A were amplified using specific primers that introduce EcoR1 and BamH1 restriction sites, ligated into the corresponding sites of ECFP-C1 or EYFP-C1 (Clontech Laboratories, Inc.). Alternatively, Xba1 and BamH1 restriction sites were introduced for ligation of U1 70K into the mammalian expression vector pCG-T7. Human HCC1.4, SRp20, and SC35 were cloned by using the cDNA cloned into the mammalian expression vector pCG-T7 as a template for PCR. Specific primers introduced BglII and BamH1 restriction sites for subsequent ligation of HCC1 into ECFP-C1 and EYFP-C1. EcoR1 and BamH1 sites were introduced for the ligation of the other constructs. SF2/ASF EGFP-C1 (a gift from G. Biamonti, Istituto di Genetica Molecolare, Pavia, Italy) was subsequently subcloned into ECFP-C1 and EYFP-C1. EGFP-SRp53 has been described previously (Cazalla et al., 2005) and was subsequently subcloned into ECFP-C1 and EYFP-C1. U2AF35 and U2AF65 in ECFP-C1 and EYFP-C1 were previously described (Chusainow et al., 2005). All constructs generated in ECFP-C1 and EYFP-C1 vectors were subcloned into EGFP-C1 (Clontech Laboratories, Inc.) and mCherry-C1 (Shaner et al., 2004). The mCherry-C1 vector was a gift from the R.Y. Tsien laboratory (University of California, San Diego, La Jolla, CA).

Cell culture and transfections
HeLa and 293T HEK cell lines were grown in DME (Invitrogen) supplemented with 10% FCS and 100 U/ml each of penicillin and streptomycin (Invitrogen) and incubated at 37°C in the presence of 5% CO_2. HeLa and 293T HEK cells were transfected with Lipofectamine 2000 (Invitrogen) according to the manufacturer's instructions.

Cell fixation and immunofluorescence microscopy
HeLa cells grown on glass coverslips were washed with PBS and fixed for 5 min in freshly prepared PBS/3.7% PFA at RT. Permeabilization was performed with PBS/1% Triton X-100 for 10 min at RT. After extensive washing, samples were blocked with 0.05% Tween 20/PBS containing 1% goat serum (Sigma-Aldrich) for at least 30 min at RT and then incubated for 1 h with the primary anti-BrdU antibody (B2531; 1:500; Sigma-Aldrich).

AMCA-conjugated goat anti–mouse secondary antibody was used at 1:500 (Jackson ImmunoResearch Laboratories) for 45 min at RT. Coverslips were then mounted in Vectashield medium (Vector Laboratories). The samples were observed on a microscope (Zeiss Axiovert-DeltaVision Image Restoration; Applied Precision, LLC).

5-FU incorporation assay
24 h after transfection, HeLa cells, either mock treated or treated with DRB for the indicated length of time, were incubated with 2 mM 5-FU (F5130) for 30 min at 37°C. Subsequently, cells were fixed, permeabilized, and incubated with primary anti-BrdU antibody (B2531; 1:500). Immunofluorescence microscopy was performed as indicated.

Western blot analysis
Samples were separated by SDS-PAGE and electroblotted Protan BA85 Nitrocellulose (Whatman) in 25 mM Tris-base, 40 mM glycine, and 20% methanol in a Genie Blotter unit (Idea Scientific Company) at 12 V for 1 h. The membranes were blocked with 1:10 Western blotting reagent (Roche) in TBST (20 mM Tris, pH 7.5, 137 mM NaCl, and 0.1% Tween 20) for 1 h at RT. Incubations with primary and secondary antibodies were performed for 1 h at RT in TBST containing 1:20 Western Blotting reagent (Roche). Four washes with TBST were done after incubations with each antibody and immunoreactive bands were detected with SuperSignal system (Thermo Fisher Scientific) according to the manufacturer's instructions. The following primary antibodies were used: mouse anti-GFP at 1:1,000 (Roche), mouse monoclonal anti-U1-70K at 1:1,000 (Synaptic Systems GmbH), rabbit anti-HCC1 at 1:5,000 (Bethyl Laboratories), mouse anti-U2AF65 at 1:200 (gift from J. Valcárcel, Centre de Regulació Genòmica, Barcelona, Spain), mAb 96 at 1:500 (for detection of SF2/ASF; Hanamura et al., 1998), and sheep anti-U2AF35 at 1:500. The appropriate secondary antibodies (HRP conjugated to IgG) were used at 1:10,000.

IP
For IP, 293T cells that were transfected with a construct expressing the protein of interest or mock transfected were resuspended in 400 µl of lysis buffer (50 mM Tris, pH 7.5, 250 mM NaCl, 5 mM EDTA, 0.5% Triton X-100, 0.3% NP-40, and 1 mM PMSF) and incubated for 10 min at 4°C. The extract was centrifuged at 12,000 g for 20 min at 4°C, after which the pellet was discarded. The extract was incubated with the antibody of choice bound to 20 µl of protein A (GE Healthcare) at 4°C for 2 h with continuous rotations. The IP reactions were then washed four times with lysis buffer. In some cases beads were treated with 50 µg/ml of RNase A/T1 cocktail (Ambion) for 10 min at 4°C after the first wash. After the washes, beads were resuspended in 30 µl of loading buffer (50 mM Tris, pH 7.5, 10% glycerol, 0.05% SDS, and 2.5% β-mercaptoethanol) and boiled for 3 min. For Western blot analysis of immunoprecipitated proteins, 10 µl of sample was used.

FRET acceptor photobleaching
HeLa cells grown on glass coverslips were cotransfected with a FRET pair of choice. 12 h after transfection, cells were mounted in Hepes-buffered Phenol red–free medium (Invitrogen) in a closed heated chamber (Bachofer). Measurements were conducted on an image restoration microscope (DeltaVision Spectris; Applied Precision) fitted with a quantifiable laser module, including a 20-mW 532-nm CW laser, suitable for photobleaching YFP without cobleaching CFP. Images were collected using a 60× 1.4 NA Plan-Apochromat lens (Olympus), a cooled charge-coupled device camera (CoolSnap HQ; Photometrics) and SoftWorx imaging software (Applied Precision, LLC). The following specific CFP/YFP filter sets were used to resolve the ECFP and EYFP signals: excitation, 436/10 nm and emission, 480/40 nm for ECFP; excitation, 525/20 nm and emission, 580/70 nm for EYFP. The dichroics used were custom built by Applied Precision, LLC and Chroma Technology, Corp. The set is modified from the normal CFP/YFP JP4 set such that the dichroic reflects and the emission filter rejects light at 532 nm, allowing this wavelength to be used for selectively photobleaching YFP. After obtaining five prebleach images, a defined region of the cell nucleus was spot photobleached with a single 150-ms stationary pulse at 90% laser power. The first image was acquired 2 ms after the bleach event. For the first second, images were acquired approximately every 200 ms, for the subsequent 1.7 s, every 335 ms, and then at 830-ms intervals in the subsequent 5 s, after which images were acquired every 1.6 s for the remainder of the experiment. A total of 20 images were acquired after the bleach event. Images of donor (ECFP) and acceptor (EYFP) were taken in separate subsequent measurements, bleaching exactly the same spot before collecting postbleach images. Obtained data were analyzed using the image analysis tools included in the SoftWorx

software and the biostatistics program Prism (GraphPad Software, Inc.). In addition to the bleached region, a similar nonbleached nuclear region in the same cell was included in the data analysis as a control. A region of background fluorescence was defined outside the cell and subtracted from both the bleached and control regions. The data were normalized against the mean intensity of the whole image over time to account for any fluctuations and normal photobleaching that occur during image acquisition throughout the course of the experiment. FRET efficiency was calculated by the following formula: FRET Efficiency = $I_{D(post)} - I_{D(pre)} / I_{D(post)}$, where $I_{D(pre)}$ and $I_{D(post)}$ are donor intensity before and after photobleaching, respectively. A FRET efficiency of >5% is considered a significant protein–protein interaction. For inhibition of transcriptional activity, cells were treated for 2 h with 25 µg/ml DRB before carrying out FRET analyses by acceptor photobleaching.

Fluorescence lifetime measurements by time-correlated single-photon counting (TCSPC) for FRET experiments
The fluorescence of organic molecules can be characterized by their excitation and emission spectra and also by the time it takes for the energized electron to return to the ground state. This is called fluorescence lifetime. When a fluorophore absorbs a photon, it enters an excited state and returns to the ground state by emitting a lower energy photon, with the energy difference between the absorbed and emitted photon transferred to the environment. One of the many factors and reactions occurring at the excited state level that can influence the measured fluorescence lifetime of a population of fluorophores is the close proximity of a second fluorescent molecule with the appropriate spectral properties to allow it to absorb energy from the first molecule through FRET (Lakowicz, 1999). Thus, FRET is a very efficient fluorescence quencher, and a decrease in the lifetime of the first (donor) fluorophore can be used to measure a FRET interaction with the second (acceptor) fluorophore. Based on these properties, FLIM provides an excellent tool for measuring differences in the lifetime of the fluorescence donor and, hence, for calculating FRET efficiencies. Furthermore, by applying a biexponential decay model we were able to resolve the fraction of the protein population that undergoes FRET (see subsequent equations in the Materials and methods and Fig. S3).

FLIM was performed using an inverted laser scanning multiphoton microscope (TE2000 [Nikon] or Radiance 2100MP [Bio-Rad Laboratories]) with a 60× oil immersion (1.4 NA). Two-photon excitation was achieved using a Chameleon Verdi-pumped ultrafast tunable (720–930 nm) laser (Coherent) to pump a mode-locked frequency-doubled Ti:Sapphire laser (Coherent) that provided sub-200-femtosecond pulses at a 90-Mhz repetition rate with an output power of ∼1.4W at the peak of the tuning curve (800 nm). Enhanced detection of the scattered component of the emitted (fluorescence) photons was afforded by the use of fast single-photon response (5783P; Hamamatsu Photonics) direct detectors. The fluorescence lifetime imaging capability was provided by TCSPC electronics (SPC-830; Becker & Hickl GmbH). TCSPC measures the time elapsed between laser pulses and the fluorescence photons. Indeed, when fluorophore molecules absorb a quantum of light, a valence electron is boosted up into a higher energy orbit, creating an excited state. When this electron returns to its original lower energy orbit (the ground state level), a quantum of light may be emitted. By consequence, the fluorescence lifetime occurs on the nanosecond time scale, and FLIM measurements reflected events occurring at an extremely short period of time. The TCSPC method used in this study is based on the detection of single photons, the measurement of the detection times of the individual photons, and the reconstruction of the waveform from the individual time measurements. Over this integration time (120 s), the waveform of the optical pulse builds up and corresponds to a histogram presenting the number of photons recorded for each nanosecond's detection time interval. Therefore, the FLIM technique provides us with the spatial map distribution of the variations of the fluorescence lifetimes and, indirectly, of the FRET efficiencies at each pixel throughout the nucleus. EGFP/mCherry was used as a FRET pair for all the FLIM measurements. The optimal two-photon excitation wavelength to excite the donor (EGFP) was determined to be 890 nm. Fluorescence emission of EGFP fusion proteins was collected using a bandpass filter (528 ± 25 nm) to limit detection to only the donor fluorophore (EGFP) and prevent contamination from the acceptor (mCherry) emission (Llères et al., 2007). Laser power was adjusted to give a mean photon count rate of the order 10^4–10^5 photons/s, and fluorescence lifetime images were acquired over 120 s. Fluorescence lifetimes were calculated for all pixels in the field of view (256 × 256 pixels) using SPCImage software (Becker & Hickl GmbH). A biexponential fluorescence decay model was applied to the data to determine the fluorescence lifetime of noninteracting and interacting subpopulations.

Analysis of the fluorescence lifetime measurements for FRET experiments

In the analysis of the FRET data, two elements must be considered: the FRET efficiency and the interacting fluorophore population. Measurements of FRET based on the analysis of the fluorescence lifetime of the donor by FLIM approach can resolve the FRET efficiency (i.e., coupling efficiency) and the FRET population (concentration of FRET species) when analyzed using biexponential decays model. The assumption that noninteracting and interacting fractions are present allows us to determine both the efficiency of the interaction and the fractional population of interacting proteins.

By applying a biexponential fluorescence decay model to fit the experimental decay curves ($f(t) = a_0 e^{+1/\tau} + a_{FRET} e^{+1/\tau_{FRET}}$) we obtain information about the lifetimes of two populations of molecules, i.e., the noninteracting donor population (lifetime τ) and the donor population that is interacting with the acceptor (lifetime τ_{FRET}), as well as the intensity factors, a_0 and a_{FRET}, of the two decay components.

By fixing the noninteracting proteins lifetime (τ) using data from control experiments (in the absence of FRET) and by assuming invariance in the efficiency of interaction (τ_{FRET}) between pixels throughout a same nuclear compartment measured (nucleoplasm or nuclear speckles domains in our study), the fraction of FRET species (i.e., population of interacting proteins) can be estimated. From this model, the FRET efficiency, E_{FRET}, can be derived from the following equation: $E_{FRET} = 1 - (\tau_{FRET} / \tau)$. A FRET efficiency of >5% is considered a significant protein–protein interaction.

Online supplemental material

Five supplemental figures are provided. They show the level of expression of the fusion proteins and their activity in alternative splicing (Figs. S1 and S2). Furthermore, use of different transcriptional inhibitors confirmed that the interactions detected by FRET/FLIM microscopy persist in the absence of transcription. Online supplemental material is available at http://www.jcb.org/cgi/content/full/jcb.200710051/DC1.

References

Blencowe, B.J., J.A. Bowman, S. McCracken, and E. Rosonina. 1999. SR-related proteins and the processing of messenger RNA precursors. *Biochem. Cell Biol.* 77:277–291.

Caceres, J.F., S. Stamm, D.M. Helfman, and A.R. Krainer. 1994. Regulation of alternative splicing in vivo by overexpression of antagonistic splicing factors. *Science.* 265:1706–1709.

Caceres, J.F., T. Misteli, G.R. Screaton, D.L. Spector, and A.R. Krainer. 1997. Role of the modular domains of SR proteins in subnuclear localization and alternative splicing specificity. *J. Cell Biol.* 138:225–238.

Caceres, J.F., G.R. Screaton, and A.R. Krainer. 1998. A specific subset of SR proteins shuttles continuously between the nucleus and the cytoplasm. *Genes Dev.* 12:55–66.

Cazalla, D., K. Newton, and J.F. Caceres. 2005. A novel SR-related protein is required for the second Step of pre-mRNA splicing. *Mol. Cell. Biol.* 25:2969–2980.

Chodosh, L.A., A. Fire, M. Samuels, and P.A. Sharp. 1989. 5,6-Dichloro-1-beta-D-ribofuranosylbenzimidazole inhibits transcription elongation by RNA polymerase II in vitro. *J. Biol. Chem.* 264:2250–2257.

Chusainow, J., P.M. Ajuh, L. Trinkle-Mulcahy, J.E. Sleeman, J. Ellenberg, and A.I. Lamond. 2005. FRET analyses of the U2AF complex localize the U2AF35/U2AF65 interaction in vivo and reveal a novel self-interaction of U2AF35. *RNA.* 11:1201–1214.

Cmarko, D., P.J. Verschure, T.E. Martin, M.E. Dahmus, S. Krause, X.D. Fu, R. van Driel, and S. Fakan. 1999. Ultrastructural analysis of transcription and splicing in the cell nucleus after bromo-UTP microinjection. *Mol. Biol. Cell.* 10:211–223.

Das, R., J. Yu, Z. Zhang, M.P. Gygi, A.R. Krainer, S.P. Gygi, and R. Reed. 2007. SR proteins function in coupling RNAP II transcription to pre-mRNA splicing. *Mol. Cell.* 26:867–881.

Day, R.N., A. Periasamy, and F. Schaufele. 2001. Fluorescence resonance energy transfer microscopy of localized protein interactions in the living cell nucleus. *Methods.* 25:4–18.

de la Mata, M., C.R. Alonso, S. Kadener, J.P. Fededa, M. Blaustein, F. Pelisch, P. Cramer, D. Bentley, and A.R. Kornblihtt. 2003. A slow RNA polymerase II affects alternative splicing in vivo. *Mol. Cell.* 12:525–532.

Dowhan, D.H., E.P. Hong, D. Auboeuf, A.P. Dennis, M.M. Wilson, S.M. Berget, and B.W. O'Malley. 2005. Steroid hormone receptor coactivation and alternative RNA splicing by U2AF(65)-related proteins CAPERalpha and CAPERbeta. *Mol. Cell.* 17:429–439.

Eperon, I.C., D.C. Ireland, R.A. Smith, A. Mayeda, and A.R. Krainer. 1993. Pathways for selection of 5′ splice sites by U1 snRNPs and SF2/ASF. *EMBO J.* 12:3607–3617.

Förster, T. 1948. Intermolecular energy migration and fluorescence. *Annalen der Physik* 437:55–75.

Fortes, P., D. Bilbao-Cortes, M. Fornerod, G. Rigaut, W. Raymond, B. Seraphin, and I.W. Mattaj. 1999. Luc7p, a novel yeast U1 snRNP protein with a role in 5′ splice site recognition. *Genes Dev.* 13:2425–2438.

Graveley, B.R. 2000. Sorting out the complexity of SR protein functions. *RNA.* 6:1197–1211.

Graveley, B.R., K.J. Hertel, and T. Maniatis. 2001. The role of U2AF35 and U2AF65 in enhancer-dependent splicing. *RNA.* 7:806–818.

Hanamura, A., J.F. Caceres, A. Mayeda, B.R. Franza, and A.R. Krainer. 1998. Regulated tissue-specific expression of antagonistic pre-mRNA splicing factors. *RNA.* 4:430–444.

Hastings, M.L., and A.R. Krainer. 2001. Pre-mRNA splicing in the new millennium. *Curr. Opin. Cell Biol.* 13:302–309.

Hastings, M.L., E. Allemand, D.M. Duelli, M.P. Myers, and A.R. Krainer. 2007. Control of Pre-mRNA Splicing by the General Splicing Factors PUF60 and U2AF. *PLoS ONE.* 2:e538.

Imai, H., E.K. Chan, K. Kiyosawa, X.D. Fu, and E.M. Tan. 1993. Novel nuclear autoantigen with splicing factor motifs identified with antibody from hepatocellular carcinoma. *J. Clin. Invest.* 92:2419–2426.

Kohtz, J.D., S.F. Jamison, C.L. Will, P. Zuo, R. Luhrmann, M.A. Garcia-Blanco, and J.L. Manley. 1994. Protein-protein interactions and 5′-splice-site recognition in mammalian mRNA precursors. *Nature.* 368:119–124.

Kramer, A. 1996. The structure and function of proteins involved in mammalian pre-mRNA splicing. *Annu. Rev. Biochem.* 65:367–409.

Lakowicz, J.R. 1999. Principles of Fluorescence Spectroscopy. Second edition. Kluwer Academic/Plenum Publishers, New York. 725 pp.

Lamond, A.I., and J.E. Sleeman. 2003. Nuclear substructure and dynamics. *Curr. Biol.* 13:R825–R828.

Lamond, A.I., and D.L. Spector. 2003. Nuclear speckles: a model for nuclear organelles. *Nat. Rev. Mol. Cell Biol.* 4:605–612.

Llères, D., S. Swift, and A.I. Lamond. 2007. Detecting protein-protein interactions in vivo with FRET using multiphoton fluorescence lifetime imaging microscopy (FLIM). *Current Protocols in Cytometry.* 42:1–19.

Listerman, I., A.K. Sapra, and K.M. Neugebauer. 2006. Cotranscriptional coupling of splicing factor recruitment and precursor messenger RNA splicing in mammalian cells. *Nat. Struct. Mol. Biol.* 13:815–822.

Maniatis, T., and R. Reed. 2002. An extensive network of coupling among gene expression machines. *Nature.* 416:499–506.

Merendino, L., S. Guth, D. Bilbao, C. Martinez, and J. Valcarcel. 1999. Inhibition of msl-2 splicing by Sex-lethal reveals interaction between U2AF35 and the 3′ splice site AG. *Nature.* 402:838–841.

Mermoud, J.E., P.T. Cohen, and A.I. Lamond. 1994. Regulation of mammalian spliceosome assembly by a protein phosphorylation mechanism. *EMBO J.* 13:5679–5688.

Mili, S., and J.A. Steitz. 2004. Evidence for reassociation of RNA-binding proteins after cell lysis: implications for the interpretation of immunoprecipitation analyses. *RNA.* 10:1692–1694.

Misteli, T. 2000. Cell biology of transcription and pre-mRNA splicing: nuclear architecture meets nuclear function. *J. Cell Sci.* 113:1841–1849.

Misteli, T., J.F. Caceres, and D.L. Spector. 1997. The dynamics of a pre-mRNA splicing factor in living cells. *Nature.* 387:523–527.

Moen, P.T. Jr., C.V. Johnson, M. Byron, L.S. Shopland, I.L. de la Serna, A.N. Imbalzano, and J.B. Lawrence. 2004. Repositioning of muscle-specific genes relative to the periphery of SC-35 domains during skeletal myogenesis. *Mol. Biol. Cell.* 15:197–206.

O'Keefe, R.T., A. Mayeda, C.L. Sadowski, A.R. Krainer, and D.L. Spector. 1994. Disruption of pre-mRNA splicing in vivo results in reorganization of splicing factors. *J. Cell Biol.* 124:249–260.

Page-McCaw, P.S., K. Amonlirdviman, and P.A. Sharp. 1999. PUF60: a novel U2AF65-related splicing activity. *RNA.* 5:1548–1560.

Patterson, G.H., D.W. Piston, and B.G. Barisas. 2000. Forster distances between green fluorescent protein pairs. *Anal. Biochem.* 284:438–440.

Phair, R.D., and T. Misteli. 2000. High mobility of proteins in the mammalian cell nucleus. *Nature.* 404:604–609.

Rappsilber, J., U. Ryder, A.I. Lamond, and M. Mann. 2002. Large-scale proteomic analysis of the human spliceosome. *Genome Res.* 12:1231–1245.

Rino, J., J.M. Desterro, T.R. Pacheco, T.W. Gadella Jr., and M. Carmo-Fonseca. 2008. Splicing factors SF1 and U2AF associate in extra-spliceosomal complexes. *Mol. Cell. Biol.* 28:3045–3057.

Robberson, B.L., G.J. Cote, and S.M. Berget. 1990. Exon definition may facilitate splice site selection in RNAs with multiple exons. *Mol. Cell. Biol.* 10:84–94.

Romfo, C.M., C.J. Alvarez, W.J. van Heeckeren, C.J. Webb, and J.A. Wise. 2000. Evidence for splice site pairing via intron definition in *Schizosaccharomyces pombe*. *Mol. Cell. Biol.* 20:7955–7970.

Sanford, J.R., J. Ellis, and J.F. Caceres. 2005. Multiple roles of arginine/serine-rich splicing factors in RNA processing. *Biochem. Soc. Trans.* 33:443–446.

Shaner, N.C., R.E. Campbell, P.A. Steinbach, B.N. Giepmans, A.E. Palmer, and R.Y. Tsien. 2004. Improved monomeric red, orange and yellow fluorescent proteins derived from *Discosoma sp*. red fluorescent protein. *Nat. Biotechnol.* 22:1567–1572.

Shen, H., and M.R. Green. 2004. A pathway of sequential arginine-serine-rich domain-splicing signal interactions during mammalian spliceosome assembly. *Mol. Cell.* 16:363–373.

Shepard, J., M. Reick, S. Olson, and B.R. Graveley. 2002. Characterization of U2AF(6), a Splicing Factor Related to U2AF(35). *Mol. Cell. Biol.* 22:221–230.

Sleeman, J., C.E. Lyon, M. Platani, J.P. Kreivi, and A.I. Lamond. 1998. Dynamic interactions between splicing snRNPs, coiled bodies and nucleoli revealed using snRNP protein fusions to the green fluorescent protein. *Exp. Cell Res.* 243:290–304.

Spector, D.L., W.H. Schrier, and H. Busch. 1983. Immunoelectron microscopic localization of snRNPs. *Biol. Cell.* 49:1–10.

Tazi, J., U. Kornstadt, F. Rossi, P. Jeanteur, G. Cathala, C. Brunel, and R. Luhrmann. 1993. Thiophosphorylation of U1-70K protein inhibits pre-mRNA splicing. *Nature.* 363:283–286.

Tronchere, H., J. Wang, and X.D. Fu. 1997. A protein related to splicing factor U2AF35 that interacts with U2AF65 and SR proteins in splicing of pre-mRNA. *Nature.* 388:397–400.

Valcarcel, J., R.K. Gaur, R. Singh, and M.R. Green. 1996. Interaction of U2AF65 RS region with pre-mRNA branch point and promotion of base pairing with U2 snRNA. *Science.* 273:1706–1709.

Wei, X., S. Somanathan, J. Samarabandu, and R. Berezney. 1999. Three-dimensional visualization of transcription sites and their association with splicing factor–rich nuclear speckles. *J. Cell Biol.* 146:543–558.

Will, C.L., and R. Luhrmann. 2001. Spliceosomal UsnRNP biogenesis, structure and function. *Curr. Opin. Cell Biol.* 13:290–301.

Wouters, F.S., P.J. Verveer, and P.I. Bastiaens. 2001. Imaging biochemistry inside cells. *Trends Cell Biol.* 11:203–211.

Wu, J.Y., and T. Maniatis. 1993. Specific interactions between proteins implicated in splice site selection and regulated alternative splicing. *Cell.* 75:1061–1070.

Wu, S., C.M. Romfo, T.W. Nilsen, and M.R. Green. 1999. Functional recognition of the 3′ splice site AG by the splicing factor U2AF35. *Nature.* 402:832–835.

Xiao, S.H., and J.L. Manley. 1997. Phosphorylation of the ASF/SF2 RS domain affects both protein-protein and protein-RNA interactions and is necessary for splicing. *Genes Dev.* 11:334–344.

Xing, Y., C.V. Johnson, P.R. Dobner, and J.B. Lawrence. 1993. Higher level organization of individual gene transcription and RNA splicing. *Science.* 259:1326–1330.

Zhang, W.J., and J.Y. Wu. 1996. Functional properties of p54, a novel SR protein active in constitutive and alternative splicing. *Mol. Cell. Biol.* 16:5400–5408.

Zorio, D.A., and T. Blumenthal. 1999. Both subunits of U2AF recognize the 3′ splice site in *Caenorhabditis elegans*. *Nature.* 402:835–838.

Zuo, P., and T. Maniatis. 1996. The splicing factor U2AF35 mediates critical protein-protein interactions in constitutive and enhancer-dependent splicing. *Genes Dev.* 10:1356–1368.